Editors' Suggestion

Imaging Fluorescence of He$_2^*$ Excimers Created by Neutron Capture in Liquid Helium II

X. Wen[1,2,3] S. R. Bao[4,5] L. McDonald[2,6] J. Pierce,[2] G. L. Greene,[1,2] Lowell Crow,[2] Xin Tong[2,7,8]
A. Mezzacappa,[1,2,9] R. Glasby,[6,9] W. Guo[4,5] and M. R. Fitzsimmons[1,2,3,*]

[1]*Department of Physics and Astronomy, University of Tennessee, Knoxville, Tennessee 37996, USA*
[2]*Oak Ridge National Laboratory, Oak Ridge, Tennessee 37830, USA*
[3]*Shull Wollan Center—A Joint Institute for Neutron Sciences, Oak Ridge, Tennessee 37830, USA*
[4]*Mechanical Engineering Department, Florida State University, Tallahassee, Florida 32310, USA*
[5]*National High Magnetic Field Laboratory, Tallahassee, Florida 32310, USA*
[6]*Department of Mechanical, Aerospace, and Biomedical Engineering, University of Tennessee, Knoxville, Tennessee 37996, USA*
[7]*Institute of High Energy Physics, Chinese Academy of Sciences (CAS), Beijing 100049, China*
[8]*Spallation Neutron Source Science Center, Dongguan 523803, China*
[9]*Joint Institute for Computational Sciences, Oak Ridge, Tennessee 37830, USA*

We show unequivocal evidence for formation of He$_2^*$ excimers in liquid He II created by ionizing radiation produced through neutron capture. Laser beams induce fluorescence of the excimers. The fluorescence is recorded at a rate of 55.6 Hz by a camera. The location of the fluorescence is determined with an uncertainty of 5 μm. The technique provides an opportunity to record the flow of He$_2^*$ excimers in a medium with very small viscosity and enables measurement of turbulence around macroscopic liter size objects or vortex matter in three dimensions.

A theoretical model that describes the development, intensity, and internal structure of turbulent flow remains an unsolved problem [1]. Direct numerical simulation of individual molecules in fluid flow has produced accepted benchmarks for canonical fluid experiments (e.g., flow over a smooth flat plate) [2] yet relies upon data of limited spatial and temporal resolution [3]. These limitations present a significant source of uncertainty [4]. Three-dimensional (3D) velocity vector field maps are required to measure the correlation of flow around macroscopic objects in space and time under conditions of large Reynolds number (Re, ratio of velocity times object dimension to kinematic viscosity of the medium). These data are required to test fundamental concepts in turbulence models applied to engineering challenges [5–7] and to enable research in quantum turbulence related to astrophysics [8] and cosmology [9].

The properties of liquid He II are modeled as a combination of superfluid and normal fluid components [10,11]. Their fractions can be controlled with temperature below the λ point [10–12]. Yet, the viscosity of liquid He II in the range of 1 to 2 K remains roughly constant $\sim 10^{-8}$ m^2/s [12–14], which simplifies modeling flow. The small viscosity and control of the velocity of the normal component using thermal gradients, i.e., thermal counterflow [10,11,15], or mechanical means [16] enable Re $\sim 10^5$ to $\sim 10^8$ to be achieved [17,18] for objects compatible with laboratory cryostats. Under steady state conditions, the mean velocity of the superfluid flow can be inferred from observation of the normal fluid flow and mass conservation [19].

The normal flow of liquid He has been observed using micrometer size polymer spheres [20,21] and frozen hydrogen particles [22,23] as tracers. Particle image velocimetry (PIV) [22,24–26] is a technique to infer flow from motion of a high density of tracers, while particle tracking velocimetry (PTV) [22,27,28] is a technique to infer flow by individually tracking tracers usually accomplished using a low density of tracers.

Recently, electric discharge from needles [29] and lasers [15,30] was used to ionize ^{4}He, which forms small "clouds" of metastable He$_2^*$ excimers. The half-life of the excimers is 13(2) s [31]. The dimensions of the clouds formed with lasers [26] or electric discharge [15] range from 10 to 800 μm, respectively. The buoyancy and small mass of the He$_2^*$ excimers mean that perturbations to flow caused by tracer clouds is significantly reduced compared to relatively massive particles. Further, excimers can be introduced into liquid He II with much less thermal heating than is associated with the introduction of massive particles. Finally, in comparison to massive particles, the binding energy of He$_2^*$ excimers to vortex cores in superfluid He is small, so the motion and configuration of vortices in quantum matter [32] should be relatively unperturbed by the excimer tracers [33].

To perform PIV or PTV requires production of He$_2^*$ excimers in varying amounts and the ability to visualize the locations of the excimer clouds to form 3D images of flow,

which remain outstanding challenges. We demonstrate a new method to produce He_2^* using neutron beams and image the excimers in 2D in a manner that is readily scalable to larger length scales and 3D. The development may enable PIV and PTV analyses of measurements of flow about centimeter size objects, which distinguishes our approach from those that produce excimers using lasers or electric discharge. In addition, hot-wire (e.g., anemometry [34]) and pressure pitot tube [35] methods enable single point measurements of flow at large Re, while our approach is also compatible with 3D visualization of the point-to-point correlation of the velocity flow field about a macroscopic object as a function of time.

A cryostat equipped with windows transparent to 640–1100 nm light cooled a liquid ^{4}He bath to 1.7 K (Fig. 1). Laser light entered the cryostat from the left-hand side (of Fig. 1); neutrons entered from the right-hand side, and the image of the fluorescence was recorded with a camera. A glass bulb measuring $1 \times 1 \times 3.6$ cm was inserted into the liquid He bath (Fig. 1 inset). The bulb was connected to a 3.5 l reservoir with a ^{3}He:^{4}He gas ratio equal to 1:241 at a pressure of 65 kPa. When liquid ^{4}He condensed in the bath, gas from the ^{3}He:^{4}He reservoir condensed inside the bulb. This configuration enabled us to explore the dependence of the fluorescence of a liquid of constant ^{3}He:^{4}He composition.

^{3}He has a large neutron capture cross section $\sigma = 16318 \times 10^{-24}$ cm^2 for $\lambda = 5.5$ Å wavelength neutrons [36,37]. Through the reaction ^{3}He $+ n \to \,^3$H $+ \,^1$H $+$ 764 keV, a triton (191 keV) and proton (573 keV) are created. These particles ionize He, which create metastable He_2^* excimers. The mean path lengths of the triton and proton in liquid He are 16 and 60 μm, respectively [38]. The energy given up by neutron capture negligibly affects the thermal energy of the liquid [39].

Laser illumination induces fluorescence of the excimers [30]. We expect the fluorescence to be proportional to the number of excimers; thus, the fluorescence is proportional to the neutron flux and λ because these factors determine the production rate of the ionizing radiation. A neutron beam with cross section 1.3×1.3 cm, $\lambda = 5.5$ Å and flux $I_0 = 10^4$ ns^{-1} cm^{-2} illuminated the helium bath.

We focused 1 kHz pulsed light of 4 ns duration/pulse and 0.9 mJ/pulse at 905 nm from a laser onto the x-z plane 1 mm wide (along y) and 10 mm tall (along z) in the center of the liquid He bath. The laser illuminated the 2 cm length of the bath (and the 1 cm length of the bulb). Owing to the transparency of liquid He to 1 μm light (absorption length $= 0.0135$ cm^{-1}), the plane is uniformly illuminated (Fig. 1).

A pulse generator produced a sequence of reference pulses ("Trigger" in the left inset of Fig. 2) with a frequency of 1 kHz. The first pulse triggered a light shutter to open at time t_1; the light shutter then closed after ~5 ms ("Light shutter" in the left inset of Fig. 2). The first, third, and fifth pulses triggered the camera to take three exposures each of 10 μs duration at a time t_2 after the preceding pulse ("Camera exposure" in the left inset of Fig. 2). A laser pulse was produced at a time t_3 after every trigger pulse ("Laser pulse" in the left inset of Fig. 2). Light from a pair of continuous wave (cw) lasers also entered the cryostat.

FIG. 1. Schematic of the equipment to excite fluorescence of He_2^* excimers. The position and time of the fluorescence is recorded with a camera. The figure is not shown to scale. The dimensions of the entire apparatus measures approximately $120 \times 75 \times 30$ cm. The camera's lateral field of view is 5×5 mm. (Inset) Schematic of the ^{3}He:^{4}He reservoir and bulb.
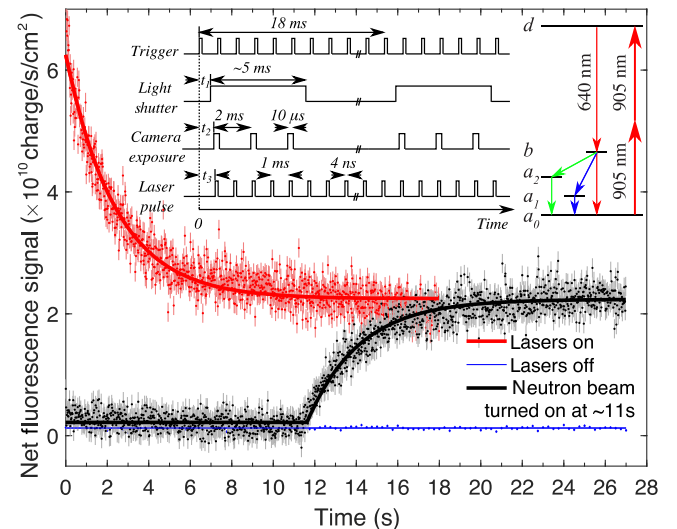
FIG. 2. (Red) Neutron beam on prior to lasers being turned on at time $= 0$. (Blue) Neutron beam on and lasers off. (Black) Lasers on (time $= 0$), neutron beam off, then turned on at time ~11 s. The bars represent 3σ errors. The solid curves are fits to functions discussed in the text. (Left inset) Timing diagram of the experiment. (Right inset) Excimer transition scheme adapted from Ref. [29].

The purpose of the light shutter was to block the cw light from unnecessarily heating the cryostat.

Through a two-step process [30], the 905 nm light excites He_2^* from its triplet ground state a_0 (right inset of Fig. 2) to an excited state d (right inset of Fig. 2) and decays via fluorescence of 640 nm light to state b (right inset of Fig. 2). The He_2^* excimer may decay back to the triplet ground state a_0 from state b or to one of two metastable vibrational states, a_1 or a_2. Excimers in metastable vibrational states cannot fluoresce until they decay into the triplet ground state—a lengthy ($\sim$2 s) process [30]. The transition time from the metastable state, a_1 or a_2, to the triplet ground state a_0 can be shortened using 1072 and 1097 nm cw lasers [31].

A camera recorded the fluorescence through a bandpass filter transparent to the 640 nm light but opaque to the infrared light. Images with pixel size ranging from 5.4 μm (1024 × 1024 pixels) to 21 μm (256 × 256 pixels) were taken over the camera's 5.5(1) × 5.5(1) mm field of view.

We quantified the influence of the laser and neutron beams and the ^{3}He number density (see the Supplemental Material [40]) to produce the fluorescence of He_2^*. Movie 1 (see the Supplemental Material [40]) shows 1000 frames collected at 55.6 Hz [Fig. 3(a)]. Each frame consists of intensity measured by 256 × 256 pixels that were mapped to the camera's field of view. The intensity profiles on the lower and right sides represent the amount of charge integrated along the direction perpendicular to the side. The quasiuniform gray color of the image is the ambient background corresponding to the gain setting of the camera and duration of the exposure. Most of the bright regions correspond to fluorescence from the clouds of excimers.

A background image was measured from the camera under conditions without laser light or neutrons. Figure 2 shows the net signal (signal image minus background image) integrated over the *entire* field of view as a function of time. To obtain the data in red (Fig. 2), (1) the bath was cooled to 1.7 K, (2) the neutron beam shutter was opened, and (3) after $\sim$4 seconds, the lasers and camera were turned on. The red curve shows the variation of the net signal with time for the conditions of the lasers and neutron

beams on. The decay of the net fluorescence signal, Z, was fitted to

$$Z(t) = Ae^{-t/\tau_1} + B, \qquad (1)$$

where t is time, τ_1 is decay time, and A and B are constants. τ_1, A, and B were adjusted to optimize the goodness of fit metric χ^2 [41]. The solid red curve is the result for $\tau_1 = 2.4(2)$ s, $A = 4.0(2) \times 10^{10}$ charge s^{-1} cm^{-2}, and $B = 2.24(4) \times 10^{10}$ charge s^{-1} cm^{-2} with $\chi^2 = 270(\chi_v^2 = 0.3)$. The net signal decays to a steady state value, B. For long time periods, there is a loss of efficiency in producing and/or detecting fluorescence. The loss may be due to some excimers being trapped in the metastable vibrational states (the a_1 and a_2 states).

The data shown in the black curve of Fig. 2 were collected starting with the lasers and camera on and the neutron beam off. At $t_0 \sim$11 s, the neutron beam shutter was opened (the shutter opens in <0.5 s). The increase of the net fluorescence signal, R, was fitted to the function that is the integral of the $e^{-t/\tau}$ portion of Eq. (1) from t_0 to t. The result is

$$R(t) = \begin{cases} C, & t < t_0 \\ D(1 - e^{-(t-t_0)/\tau_2}) & t \geq t_0 \end{cases} \qquad (2)$$

for $\tau_2 = 2.8(3)$ s, $C = 2.2(4) \times 10^9$ charge s^{-1} cm^{-2}, and $D = 2.02(6) \times 10^{10}$ charge s^{-1} cm^{-2} for $\chi^2 = 188(\chi_v^2 = 0.2)$. C represents an underestimate of the background used in subtraction from the raw image. $B \sim C + D$; thus, the strength of the fluorescence at steady state is nearly the same for the two protocols. The variation of the black data from zero (neutron beam off) to a nonzero value (neutron beam on) shows that the neutron capture of the ^{3}He:^{4}He mixture is a necessary condition to produce fluorescence. The blue curve of Fig. 2 shows the net signal integrated over a long camera exposure time for the case of the neutron beam on and the lasers off. These data indicate the need for laser illumination to observe their fluorescence.

Focusing on the red data in Fig. 2, the decay of the signal can be understood in terms of the neutron beam first creating a large abundance of He_2^* excimers, which primarily occupy the a_0 triplet ground state, because the lasers are not yet on. The concentration of excimer clouds can be estimated at $A_0 \sim 10^4$ clouds/cm^3 from the beam flux, the time of a few seconds (4 s) prior to turning on the lasers, and the volume of the bulb. The excimers are confined to the liquid inside the bulb. Because the neutron absorption length of 0.4% ^{3}He in liquid ^{4}He is large $\mu = 2$ cm^{-1} for $\lambda = 5.5$ Å, 63% of the excimer production occurs in the region of the bulb *outside the field of view* of the camera as the neutron beam enters the bulb. Twenty-three percent of the exciter production occurs inside the field of view.
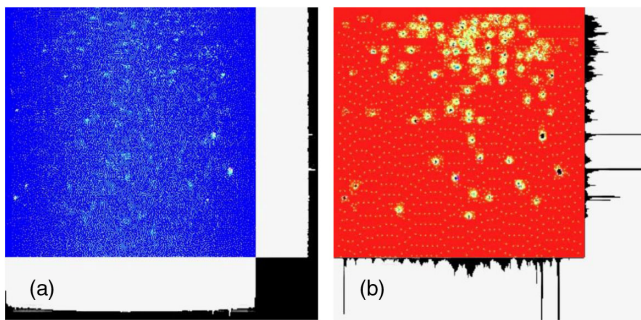
FIG. 3. Screenshots of the first image of (a) Movie 1 (the raw movie) and (b) Movie 2 (interpreted from the peak finding algorithm). See the Supplemental Material [40].

Next, the lasers were turned on to produce fluorescence of the excimers. For the conditions of our experiment, we find that the steady state fluorescence signal is ~33% of the maximum. The steady state value is achieved about 2.4(2) s after the lasers are turned on.

Focusing on the black data in Fig. 2, the increase of the signal can be understood in terms of the absence of excimers ($A_0 = 0$ excimers/cm^3) before the neutron beam is turned on. Once the neutron beam is turned on, He$_2^*$ excimers are created, and in the presence of laser light they fluoresce. With time, more excimers are created, yet because the fluorescence achieves a steady state, there must be competition between the production of excimers capable of fluorescence (those in the a_0 state) and loss of these excimers. Equation (2) represents the strength of the fluorescence at time $t > t_0$ from the superposition of excimers created from time t_0 (neutron beam on) to time t that decay with the timescale of $\tau_2 = 2.8(3)$ s.

Because only the initial conditions of the two protocols (red, neutron exposure before laser illumination; black, laser illumination before neutron exposure) were changed (i.e., ^{3}He concentration was constant, neutron flux was constant, etc.), we expect the two protocols to achieve the same steady state values. Further, because the steady state value is controlled by the rate that active excimers are lost, the decay times (τ_1 and τ_2) for the two protocols should be the same. The steady state values achieved by the red and black data in Fig. 2 ($B \sim C + D$) might have been increased had the decay time been longer.

From the movies [an example is Movie 1 [Ref. [40], Fig. 3(a)], we quantified the intensities, sizes, and positions of the excimer clouds as a function of time. Clouds of fluorescence consist of charge recorded by the camera in a region of pixels numbering from one to several. Because the charge integrated over the field of view is dominated by background and not the occasional fluorescence, the mean of the entire measurement, ϕ, and the standard deviation above the mean, σ, were used to quantify the background. Events with peak intensity 3σ greater than ϕ were identified. For data recorded from an exposure with 1024×1024 pixels, approximately 2000 events per frame were identified, and about 70% of these correspond to clusters of two or more pixels. In a region of interest that was stepped across an image, the center of mass (c.m.) of a single event or cluster, the standard deviation of the c.m., $\sigma_{c.m.}$, and the net charge of the cluster (i.e., charge greater than ϕ) integrated within $2\sigma_{c.m.}$ of the c.m. were computed for each event or cluster. The number of events versus net charge integrated over the duration of the exposure is shown in Fig. 4(a) (single pixel events are shown in gray). The size distribution of clusters corresponding to two or more events (numbering 90 725) in close spatial proximity (but not in the same pixel) and occurring at the same time is shown in Fig. 4(b). The average of the size distribution is 25(3) μm. This average is within the range of 10 to 60 μm expected from the mean free path of tritons and protons
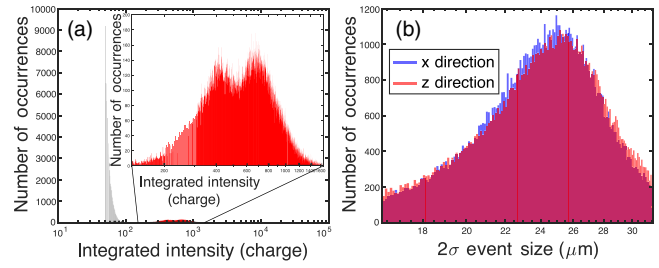
FIG. 4. Distributions of (a) integrated intensity and (b) size of events. Data are recorded in a field of view mapped to 1024×1024 pixels in 50 exposures of 10 μs each.

in liquid He and may represent a dimension characteristic of a cluster of He$_2^*$ excimers.

The image for the nth frame corresponding to fluorescence (without background) was formed by summing events within $2\sigma_{c.m.}$ of the c.m. of each event or cluster from Movie 1 [40]. The sequence of these images constitutes Movie 2 [see the Supplemental Material [40] and Fig. 3(b)]. Movie 2 [40] represents only the fluorescence that fulfills our discrimination criterion and should reveal the velocity field through the values of the c.m.'s corresponding to He$_2^*$ excimer tracer clouds. These values are needed to obtain the velocity flow of the tracers with particle tracking algorithms.

In summary, we demonstrated the ability to create numerous He$_2^*$ excimers corresponding to an excimer cloud density of 10^4/cm^3 in a ~4 cm^3 volume of liquid He. Owing to the small binding energy of the excimers on quantized vortices, excimer clouds follow the motion of the viscous normal fluid in He II, thereby allowing observation of turbulence resulting from mutual friction with the superfluid component [33]. At temperatures below about 0.6 K where the excimers can bind to vortices [32], our method may provide a nonintrusive way to introduce excimer tracers into pure superfluid for vortex imaging. The fluorescence from the excimers was recorded as images of clouds measuring ~25(3) μm in diameter and numbering ~34 per image in a 0.03 cm^3 volume defined by the camera's field of view and the 1 mm thickness of the focal plane illuminated by the lasers. This calculation suggests ~10% of the excimer production contributed toward excimer fluorescence. From Movie 2 [40], the sample density (of fluorescence from clouds or clusters of He$_2^*$ excimers) in the region across the camera's field of view in the focal plane was approximately one per mm^2. The uncertainty in the extraction of the positions of centroids of the events, i.e., the spatial resolution of the technique, was ~5 μm. In order to measure flow of Re $\sim 10^5$ for a centimeter size object in liquid He from frames separated in time by 18 ms would require tracking an excimer cloud across a separation of 2 mm—a separation too large to consider such a pair of events as being produced by the same excimer cloud.

Looking to the future, we offer perspectives on how to improve the technique. From the physics perspective, the steady state rate is presently limited by the loss of excimers that are able to fluoresce. The decay time of ∼3 s is much less than the 13 s half-life of the excimer; therefore, it may be possible to increase the steady state value of the fluorescence by 4×, e.g., using higher power repumping lasers. Success might allow the technique to be implemented with portable neutron sources instead of a neutron facility, and also the possibility of increasing the sample density to one per 0.25 mm^2.

The hydrodynamics of liquid He II is controlled by phonon and roton excitations—the latter dominate at 1.7 K—and the interactions of the excitations with impurities [42]. For our experiment, the mass density of ^{3}He atoms is 0.0003 g/cm^3, while the mass density of rotons at 1.7 K is 0.033 g/cm^3 [14]. Because the mass density of ^{3}He is only 0.1% that of the rotons, we do not expect the presence of ^{3}He to affect the hydrodynamics.

From the technical perspective, the spatial and temporal resolutions are limited by the speed of the camera and the lack of a large fast buffer to store data. With relatively straightforward improvements to the equipment, the spatial resolution can be improved from 5 to ∼1 μm, and the time between exposures can be reduced from 18 to 1 ms. Finally, with the addition of a second set of lasers and a second camera, a second plane of fluorescence can be imaged to visualize flow in 3D.

*Corresponding author.
mf3@ornl.gov

[1] I. Eames and J. B. Flor, New developments in understanding interfacial processes in turbulent flows, Phil. Trans. R. Soc. A **369**, 702 (2011).

[2] P. Lammers, K. N. Beronov, R. Volkert, G. Brenner, and F. Durst, Lattice BGK direct numerical simulation of fully developed turbulence in incompressible plane channel flow, Comput. Fluids **35**, 1137 (2006).

[3] P. K. Yeung, K. R. Sreenivasan, and S. B. Pope, Effects of finite spatial and temporal resolution in direct numerical simulations of incompressible isotropic turbulence, Phys. Rev. Fluids **3**, 064603 (2018).

[4] T. A. Oliver, N. Malaya, R. Ulerich, and R. D. Moser, Estimating uncertainties in statistics computed from direct numerical simulation, Phys. Fluids **26**, 035101 (2014).

[5] F. G. Schmitt, About Boussinesq's turbulent viscosity hypothesis: Historical remarks and a direct evaluation of its validity, C.R. Mec. **335**, 617 (2007).

[6] L. Prandtl, Report on investigation of developed turbulence, Z. Angew. Math. Mech. **5**, 136 (1925).

[7] J. Smagorinsky, General circulation experiments with the primitive equations, Mon. Weather Rev. **91**, 99 (1963).

[8] D. Page, M. Prakash, J. M. Lattimer, and A. W. Steiner, Rapid Cooling of the Neutron Star in Cassiopeia A Triggered by Neutron Superfluidity in Dense Matter, Phys. Rev. Lett. **106**, 081101 (2011).

[9] C. Bäuerle, Yu. M. Bunkov, S. N. Fisher, H. Godfrin, and G. R. Pickett, Laboratory simulation of cosmic string formation in the early Universe using superfluid ^{3}He, Nature (London) **382**, 332 (1996).

[10] W. F. Vinen, The physics of superfluid helium in *Proceedings of the CASCERN Accelerator School on Superconductivity and Cryogenics for Accelerators and Detectors, Erice, Italy,2002* edited by S. Russenschuck and G. Vandoni (CERN Report No. CERN-2004-008, 2004), pp. 363–373.

[11] W. F. Vinen, An introduction to quantum turbulence, J. Low Temp. Phys. **145**, 7 (2006).

[12] J. G. Dash and R. D. Taylor, Hydrodynamics of oscillating disks in viscous fluids: Density and viscosity of normal fluid in pure He^4 from 1.2 K to the lambda point, Phys. Rev. **105**, 7 (1957).

[13] J. T. Tough, W. D. McCormick, and J. G. Dash, Viscosity of liquid He II, Phys. Rev. **132**, 2373 (1963).

[14] R. J. Donnelly and C. F. Barenghi, The observed properties of liquid helium at the saturated vapor pressure, J. Phys. Chem. Ref. Data **27**, 1217 (1998).

[15] W. Guo, S. B. Cahn, J. A. Nikkel, W. F. Vinen, and D. N. McKinsey, Visualization Study of Counterflow in Superfluid ^{4}He using Metastable Helium Molecules, Phys. Rev. Lett. **105**, 045301 (2010).

[16] P. M. McConnell, *Liquid helium pumps*, NBS Interim Report No. NBSIR 73-316 (National Bureau of Standards, Gaithersburg, MD, 1973).

[17] R. J. Donnelly and K. R. Sreenivasan, *Flow at Ultra-High Reynolds and Rayleigh Numbers: A Status Report* (Springer-Verlag, New York, 1998).

[18] R. J. Donnelly, *High Reynolds Number Flows Using Liquid and Gaseous Helium* (Springer-Verlag, New York, 1991).

[19] M. E. Hayden, G. Archibald, P. D. Barnes, W. T. Buttler, D. J. Clark, M. D. Cooper, M. Espy, R. Golub, G. L. Greene, S. K. Lamoreaux, C. Lei, L. J. Marek, J.-C. Peng, and S. I. Penttila, Neutron-Detected Tomography of Impurity-Seeded Superfluid Helium, Phys. Rev. Lett. **93,** 105302 (2004).

[20] T. Zhang and S. W. Van Sciver, Large-scale turbulent flow around a cylinder in counterflow superfluid ^{4}He (He (II)), Nat. Phys. **1,** 36 (2005).

[21] T. Zhang, D. Celik, and S. W. Van Sciver, Tracer particles for application to PIV studies of liquid helium, J. Low Temp. Phys. **134,** 985 (2004).

[22] J. Xu, K. M. Smith, D. Celik, M. Y. Hussaini, and S. W. Van Sciver, Hydrogen particles in liquid helium, Cryogenics **44,** 507 (2004).

[23] G. P. Bewley, K. R. Sreenivasan, and D. P. Lathrop, Particles for tracing turbulent liquid helium, Exp. Fluids **44,** 887 (2008).

[24] M. Raffel, C. E. Willert, F. Scarano, C. J. Kähler, and S. T. Wereley, *Particle Image Velocimetry—A Practical Guide* (Springer, Berlin, 2007).

[25] R. J. Donnelly, A. N. Karpetis, J. J. Niemela, K. R. Sreenivasan, W. F. Vinen, and C. M. White, The Use of particle image velocimetry in the study of turbulence in liquid helium, J. Low Temp. Phys. **126,** 327 (2002).

[26] W. Guo, M. La Mantia, D. P. Lathrop, and S. W. Van Sciver, Visualization of two-fluid flows of superfluid helium-4, Proc. Natl. Acad. Sci. U.S.A. **111,** 4653 (2014).

[27] T. Dracos, Particle tracking velocimetry (PTV) in *Three-Dimensional Velocity and Vorticity Measuring and Image Analysis Techniques ERCOFTAC Series 4*, edited by T. Dracos (Springer, Dordrecht, 1996), pp. 155–160.

[28] B. Sokoray-Varga and J. Józsa, Particle tracking velocimetry (PTV) and its application to analyse free surface flows in laboratory scale models, Periodica polytechnica: Civil engineering Bauingenieurwesen **52,** 63 (2008).

[29] W. Guo, J. D. Wright, S. B. Cahn, J. A. Nikkel, and D. N. McKinsey, Metastable Helium Molecules as Tracers in Superfluid ^{4}He, Phys. Rev. Lett. **102,** 235301 (2009).

[30] A. Marakov, J. Gao, W. Guo, S. W. Van Sciver, G. G. Ihas, D. N. McKinsey, and W. F. Vinen, Visualization of the normal-fluid turbulence in counterflowing superfluid ^{4}He, Phys. Rev. B **91,** 094503 (2015).

[31] W. G. Rellergert, S. B. Cahn, A. Garvan, J. C. Hanson, W. H. Lippincott, J. A. Nikkel, and D. N. McKinsey, Detection and Imaging of He$_2$ Molecules in Superfluid Helium, Phys. Rev. Lett. **100,** 025301 (2008).

[32] D. E. Zmeev, F. Pakpour, P. M. Walmsley, A. I. Golov, W. Guo, D. N. McKinsey, G. G. Ihas, P. V. E. McClintock, S. N. Fisher, and W. F. Vinen, Excimers He$_2^*$ as Tracers of Quantum Turbulence in ^{4}He in the $T = 0$ Limit, Phys. Rev. Lett. **110,** 175303 (2013).

[33] W. Guo, Molecular tagging velocimetry in superfluid helium-4: Progress, issues, and future development, J. Low Temp. Phys. **196,** 60 (2019).

[34] M. Hultmark, M. Vallikivi, S. C. C. Bailey, and A. J. Smits, Turbulent Pipe Flow at Extreme Reynolds Numbers, Phys. Rev. Lett. **108,** 094501 (2012).

[35] S. C. C. Bailey, M. Hultmark, J. P. Monty, P. H. Alfredsson, M. S. Chong, R. D. Duncan, J. H. M. Fransson, N. Hutchins, I. Marusic, B. J. McKeon, H. M. Nagib, R. Örlü, A. Segalini, A. J. Smits, and R. Vinuesa, Obtaining accurate mean velocity measurements in high Reynolds number turbulent boundary layers using Pitot tubes, J. Fluid Mech. **715,** 642 (2013).

[36] S. Falahat, A. Best, M. Couder, J. Görres, K. Kratz, U. Ott, E. Stech, and M. Wiescher, A ^{3}He neutron detector for the measurement of (α, n) reactions, Nucl. Instrum. Methods Phys. Res., Sect. A **700,** 53 (2013).

[37] A. Rauch and W. Waschkowski, Neutron properties in *Neutron Data Booklet*, edited by A.-J. Dianoux and G. Lander (Institut Laue-Langevin, Grenoble, 2002), pp. 1.1–4.

[38] C. F. Williamson, J. P. Boujot, and J. Picard, Tables of range and stopping power of chemical elements for charged particles of energy 0.05 to 500 MeV, Centre D'Etudes Nucleaires de Saclay Report No. CEA-R3042, 1966, pp. 3–151.

[39] M. J. Buckingham and W. M. Fairbank, The nature of the λ-transition in liquid helium, Prog. Low Temp. Phys. **3,** 80 (1961).

[40] See Supplemental Material at http://link.aps.org/supplemental/10.1103/PhysRevLett.124.134502 for further details on experimental methods, movies, and the influence of neutron flux and the quantity of ^{3}He on the net fluorescence signal.

[41] W. H. Press *et al.*, *Numerical Recipes: The Art of Scientific Computing* (Cambridge University Press, Cambridge, England, 1986), p. 470.

[42] T. M. Sanders, Jr., Semiclassical mechanics of rotons, Contemp. Phys. **42,** 151 (2001).